The Influence of Minor Elements on the Weldability of an INCONEL 718–Type Superalloy

S. BENHADAD, N.L. RICHARDS, and M.C. CHATURVEDI

The effect of the minor elements C, B, and P on the weldability of the INCONEL 718 alloy was studied. Wrought alloys containing systematic additions of the three minor elements were evaluated by thermal simulation and by electron-beam welding. The ductility recovery temperature from the thermal simulation experiments and the microfissuring behavior in the heat-affected zone (HAZ) of the electron-beam samples were used to evaluate the effect of minor elements on weldability.

Carbon was found to have minimal effect on weldability, whereas, as previously observed, B has a significant negative impact on weldability. The element P, in combination with B, was extremely detrimental to weldability, but C mitigated the harmful effects of B and P, both individually and in combination. The effect of the minor-element additions has been explained in terms of site competition of segregating species on grain boundaries.

I. INTRODUCTION

INCONEL* 718 is the most widely used superalloy in the aerospace industry, with good mechanical properties up to 650 °C. It is, however, susceptible to intergranular heat-affected-zone (HAZ) cracking during welding. A great deal of research has been carried out to solve this problem. The research conducted in the 1960s[1] attributed it to the liquation of MC carbides at the grain boundaries (GBs) or to the liquation of GBs due to the segregation of melting-point-suppressing elements on them. In the 1980s and 1990s, research by Thompson and co-workers[2,3,4] and statistical work by Kelly[5] showed that minor elements can cause precipitates to form on GBs, which may undergo constitutional liquation during welding, resulting in HAZ microfissuring. In superalloys, while P has been reported to be harmful,[6] the effect of C has been observed to be either detrimental[2] or innocuous.[5] In the INCONEL 718 superalloy, Thompson favored S as the main problem element, whereas Kelly suggested B to be the main cause of cracking of welds. Subsequent work by the present authors[7,8,9] on cast INCONEL 718 *via* secondary ion mass spectrometry (SIMS) analysis showed that only elemental segregation of B on GBs appeared to cause the microfissuring. They also concluded that B can segregate to GBs during prewelding solution heat treatment by equilibrium segregation mechanisms and during subsequent cooling by a nonequilibrium segregation mechanism. It has been established that the equilibrium segregation depends on the solution heat-treatment temperature and increases with a decrease in temperature. The nonequilibrium segregation, however, depends upon the cooling rate from the solution heat-treatment temperature. Later on, the research by the present authors on INCONEL 718–based alloys with controlled additions of B and S showed that while S can cause HAZ microfissuring, the detrimental effect of B is far more severe.[10] However, the influence of the combined addition of C, B, and P on the HAZ microfissuring behavior of INCONEL 718 has not been studied.

With the aim to improve on existing mechanical properties, the nominal composition of INCONEL 718 has been modified by minor additions of several elements such as C, B, and P by various researchers. Recently, Cao and Kennedy[11] have proposed a very significant increase in B and P concentrations, with optimum high-temperature properties provided by the addition of 0.022 pct P and 0.011 pct B. The weldability of this alloy has not been reported, but, based on the authors' earlier studies, it should be influenced by the tendency of B and P to segregate to the GBs during the preweld heat treatment. It has been observed in many alloys that elements like C, B, and P influence the tendency of each other to segregate to GBs. For example, Guttmann,[12] and also Erhart and Grabke,[13] through a systematic analysis of plain-carbon and chromium-alloy steel, showed that the presence of C reduced the segregation of P at the austenite grain boundaries through site competition between the elements. Similarly, Paju *et al.*[14,15,16] have shown equivalent behavior in Fe-P, Fe-P-C, and Fe-Mn-C-P alloys, where B reduced the segregation of P, with no enhancement of P segregation by Cr, Mn, Ni, or V additions. (For a more complete discussion, the reader is referred to the authors' review article on the subject.[17]) Therefore, it is likely that the segregation of C, B, and P in the modified INCONEL 718 proposed by Cao and Kennedy may also depend on the concentration of these elements and their interactions with each other and should influence their weldability. Therefore, research was initiated to study the weldability of these alloys. The present communication presents the effect of controlled additions of C, B, and P, individually and in combination, on the weldability of INCONEL 718–type alloys.

*INCONEL is a trademark of INCO Alloys International, Huntington, WV.

S. BENHADAD, Senior Research Scientist, is with Global Thermoelectric Inc., Calgary, AB, Canada T2B 3R2. N.L. RICHARDS, Associate Professor, and M.C. CHATURVEDI, Professor, are with the Department of Mechanical and Industrial Engineering, University of Manitoba, Winnipeg, MB, Canada R3T 5V6. Contact e-mail: mchat@cc.umanitoba.ca

Manuscript submitted August 30, 2000.

Table I. Concentration of C, P, and B in Various IN718 Base Alloys

Alloy	C (Wt Pct)	B (Wt Pct)	P (Wt Pct)
(Base)	0.008	<0.001	<0.001
(Base + C)	0.031	<0.001	<0.001
(Base + B)	0.005	0.013	<0.001
(Base + C + B)	0.031	0.012	<0.001
Base + B + P	0.006	0.010	0.022
(Base + C + P)	0.030	<0.001	0.022
(Base + B + C + P)	0.033	0.011	0.022

II. EXPERIMENTAL METHODS AND MATERIALS

Hot-rolled bars (16.0 mm in diameter) of INCONEL 718–type alloys with varying B, C, and P concentrations (Table I) were provided by Allvac. The composition of the base alloy (in wt pct) was 53.16 pct Ni, 19.38 pct Fe, 17.8 pct Cr, 2.87 pct Mo, 5.06 pct Nb + Ta, 0.92 pct Ti, 0.63 pct Al, 0.10 pct Si, 0.031 pct C, 0.004 pct B, 0.006 pct P, 0.0017 pct Mg, 0.0037 pct N, and 0.0004 pct S). The as-received bars had the following processing history: (1) vacuum induction melted (VIM) cast: 23 kg ingots of 70 mm in diameter; (2) vacuum arc refined (VAR) cast: 100-mm-diameter ingots; (3) homogenized: 1190 °C for 16 hours; and (4) the ingots were rolled to 16.5-mm-diameter bars between 1040 °C and 920 °C.

The as-received bars were cold swaged in two steps, with two intermediate anneals of 1 hour each at 1200 °C and 1050 °C, to produce rods suitable for testing in a Gleeble thermal simulator. The specimens were given a final solution heat treatment at 1050 °C for 45 minutes, followed by two cooling rates, *viz.*, air cooling at 11°C/s and water quenching at 284 °C/s. The solution treatment at 1050 °C eliminated the complexity of having the delta phase in the microstructure, *i.e.*, a clean microstructure was present apart from some primary carbides and occasional nitrides. Aging was not carried out, since, normally, components are welded in the solution-treated condition.

After normal metallographic preparation, the microstructure of the heat-treated specimens was characterized by a JEOL* JSM-5900LV scanning electron microscope (SEM) with Oxford energy-dispersive spectroscopy X-ray analysis capability (SEM/EDS). Transmission electron microscope (TEM) analysis of carbon extraction replicas was carried out on a JEOL 2000FX microscope operating at 200 kV. Grain-boundary segregation was examined by SIMS. An O_2^+ primary ion beam was used to investigate the presence of B as the molecular secondary ion beam $^{10}B^{16}O_2$, and a Cs^+ primary ion beam was used for the investigation of C present as the molecular secondary ion C_2^-. The same Cs^+ primary ion beam was used for the investigation of P.

*JEOL is a trademark of Japan Electron Optics Ltd., Tokyo.

The hot ductility of the heat-treated specimens was measured by a Gleeble 1500 thermal-mechanical simulator. Round test pieces 115-mm long and 6 mm in diameter, with threaded ends, were held between Cu grips, the threaded end being held in stainless steel holders. A heating rate of 150 °C/s and a strain-rate value of 0.4 s^{-1} was used, and testing was carried out in argon. During the tests, the samples were thermally cycled up to a peak temperature (T_p) of 1210 °C. This temperature had been shown by previous experimentation to give a reasonable amount of liquated phase at the grain boundaries. Test pieces were then held at 1210 °C for 5 seconds before cooling to the test temperature, held for 5 seconds at the test temperature, and then tested, with usually a 25 °C interval between tests. The hot ductility of the material at the test temperature was estimated on a broken specimen by the measurement of the reduction of area from three test samples.

Besides the thermal simulation carried out on the Gleeble system, electron-beam welding was performed on a MarkVII Sciaky welder with beam parameters of 40 kV and 30 mA, a travel speed of 77 cm/min, and a sharp focus. The weldability of alloys was estimated by measuring the length of cracks found in the HAZ and reported as the average total crack length per section (Av. TCL). Cross sections of the welds were cut, polished, and etched before performing the measurement of crack length on the SEM using the IPP software by NORAN.

III. RESULTS

A. *Microstructural Analysis*

Figure 1(a) shows a SEM micrograph of the base alloy in the air-cooled (AC) condition. The alloy's microstructure was essentially single-phase austenite with a mean linear-intercept grain size of about 90 μm. Within the microstructure, there were randomly dispersed MC-type carbides, with a round-to-blocky morphology. The EDS analysis of the precipitates (Table II) showed them to be mainly Nb-rich MC carbides containing some Ti; in addition, the EDS spectrum showed a small amount of B in the carbide, as well as the C peak. Due to the software limitations, it was not possible to quantify the B and C concentrations. The TEM analysis of these particles extracted on carbon replicas (Figure 1(b)) revealed them to correspond to MC-type particles with an fcc crystal structure and a lattice parameter of 0.45 nm. The selected-area diffraction patterns (SADPs) were indexed from the [001], [110], and [111] zone axes, with the [001] pattern being shown in Figure 1(c). Similarly, the microstructure of the base + C alloy after air cooling, as well as after water quenching, was essentially the same as that of the base alloy, except more carbides were observed; in addition, a few TiN precipitates were also observed, some acting as nuclei for the MC carbide.

The addition of B to the base + C alloy resulted in the microstructure containing two types of precipitates, although the general microstructure was similar to the base alloy. One of the precipitate types was the fcc Nb-rich carbide containing B (Figures 2(a) through (c)), as was observed in the base alloy and the C-containing alloy. Figure 2(a) shows the Nb-rich precipitate, with the associated X-ray maps of boron and carbon shown in Figures 2(b) and (c), respectively. The EDS spectrum revealing B and C in the precipitate is shown in Figure 2(d). The second precipitate type was rich in Nb, Mo, and CR, as shown in Table II. These latter particles were also extracted on carbon replicas, and a representative TEM micrograph is shown in Figure 3(a). The morphology of precipitates varied from approximately round to oval (aspect ratio about 2:1), the round ones being from about 200 to 500 nm in size. The analysis of SADPs from these particles, an example of which in the [001] orientation

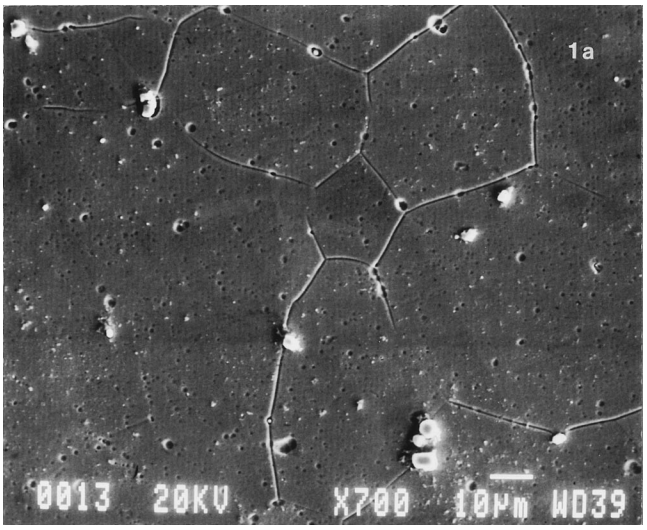

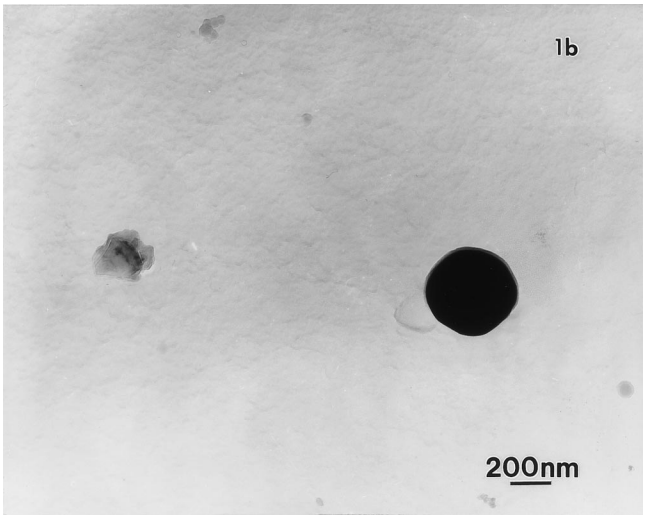

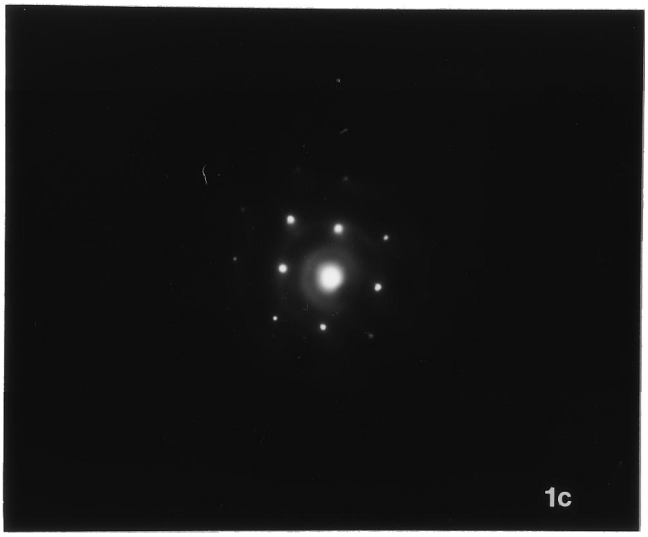

Fig. 1—Micrographs of air-cooled base alloy: (*a*) SEM micrograph showing equiaxed microstructure and blocky MC carbides at both intra- and intergranular locations; (*b*) TEM image of Nb-rich Ti containing MC carbide in the carbon extraction replica; (*c*) SAD pattern with [001] zone axis of MC carbide shown in (b).

Table II. TEM/EDX Analysis of Precipitates in Atomic Percent

Precipitate		Nb	Ti	Ni	Cr	Mo	Fe	P
NbTiC(B)	average	81	16	1	0.5	1	1	—
	range	74/83	14/19	0/1	0/1	1/2	1/2	—
TiNbC	average	6	92	0.5	0.5	1	0	—
	range	2/10	88/97	0/2	0/1	1/2	0	—
NbMoCr boride	average	38	1	2	24	30	5	—
	range	33/40	0.5/1.0	1.5/2.5	23/25	26/36	4/6	—
Vincent[18]—boride	range	37/44	1/3	2/11	22/27	10/35	3/5	—
NbTiCrC	average	66	23	0.25	8	2	0.2	—
	range	63/69	18/28	0.1/0.3	1/15	1/3	0/0.5	—
NbNiTiCrFeC	average	57	8	17	7	4	7	—
NbNiCrFeC	average	37	5	30	12	3	10	3

is shown in Figure 3(b), revealed them to be tetragonal M_3B_2 particles with lattice parameters of $a = 0.57$ nm and $c = 0.22$ nm. The crystal structure and lattice parameters of these particles is similar to that observed by Vincent[18] in the HAZ of INCONEL 718.

The alloy containing both C and B additions also had the same general microstructure as the previous alloys, with Nb-rich carbide particles containing B, along with some Ti-rich carbides; the Ti-rich carbides also contained Nb (Table II). The EDS spectra revealed the presence of both C and B in

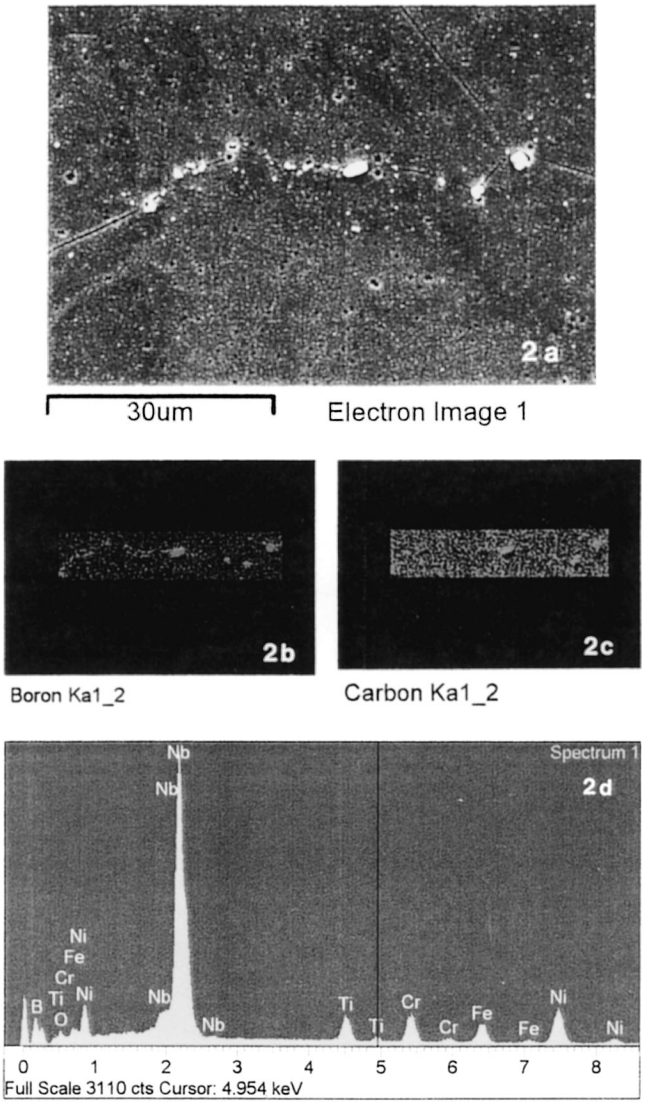

Fig. 2—(*a*) SEM micrograph of the base + B alloy showing Nb rich grain boundary carbides, (*b*) associated X-ray map for C, (*c*) X-ray map of B, and (*d*) EDS spectrum of carbide in (a) showing B and adjacent C peaks.

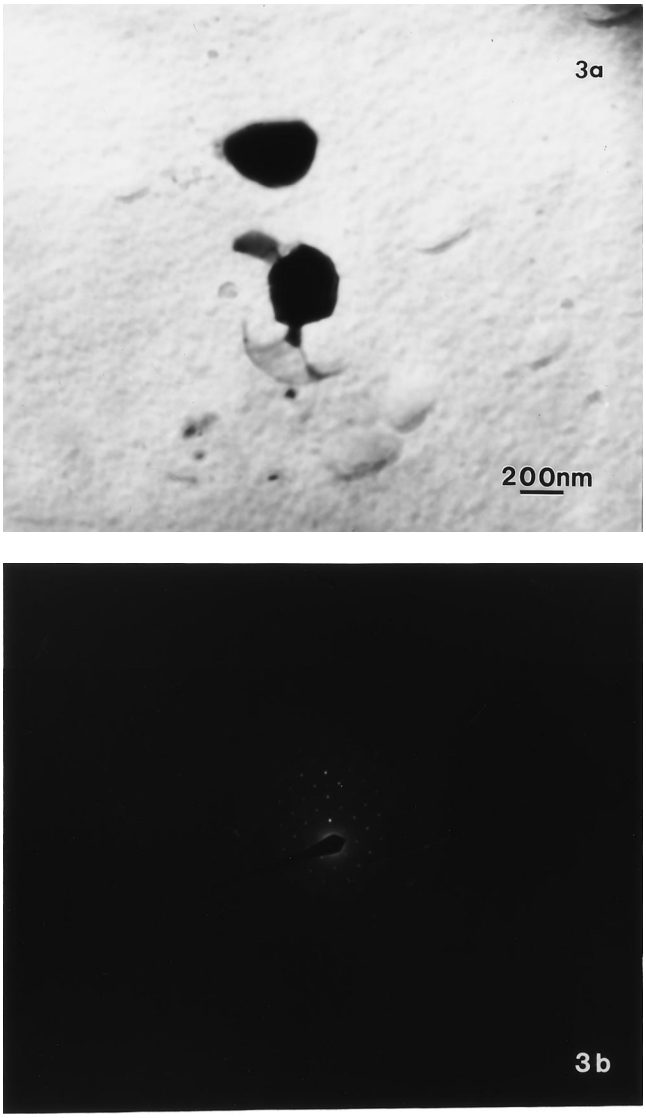

Fig. 3—(*a*) TEM micrograph of an extraction replica of base + B alloy showing M_3B_2 particle and (*b*) its SAD pattern in[001] zone axis.

the precipitates, but the M_3B_2 Nb/Mo/Cr/Fe tetragonal boride was not observed in this alloy. Figure 4(a) shows an SEM micrograph. The X-ray maps of B and C in an MC carbide, plus a section of the spectrum indicating the presence of B and C, are shown in Figures 4(b) through (d), respectively. Again, the MC carbide was round to cuboidal in shape. The absence of the boride phase was corroborated by the TEM analysis, where only MC carbide (Figures 5(a) and (b)) with a lattice parameter of 0.45 nm was observed.

The B + P alloy showed similarities to the B-containing alloy, with Nb-rich B containing carbide precipitates and also borides. However, some P (up to 5 at. pct) was also observed in a few Nb/Ni/Cr/Fe-containing carbide particles that were present in this alloy (Table II). In addition, 15 to 20 pct of the precipitates examined were of M_3B_2-type borides, having a composition similar to that observed in precipitates in the base + B alloy. Figure 6(a) shows an SEM image of a collection of round and irregularly shaped Nb/Mo/Cr/Fe boride particles on a grain boundary, and the X-ray maps for B and C from selected areas of the agglomerate are shown in Figures 6(b) and (c), respectively. Figure 6(d) shows the EDS spectrum from one of the precipitates. In addition, some mainly round Ti-rich carbides, with less than 5 pct of the other elements in them, were also observed.

As with the microstructures of all the alloys, the two remaining alloys (the base + C + P and base + B + C + P alloys) also exhibited the same general basic austenitic microstructure. The primary precipitate in the base + C + P alloy contained mainly Nb-rich carbide particles of varying sizes, again similar to the base alloy. Some B was also observed in the EDS spectra of some precipitates, even though the alloy bulk B concentration was below 0.001 wt pct. In addition, minor amounts of a round/cuboidal Nb/Ni/Ti/Cr/Fe-rich phase (Figure 7(a)) were also observed, with the analysis shown in Table II. From the TEM micrograph (Figure 7(b)) and the SADP analysis (Figure 7(c)), the precipitates were indexed to be fcc, with a lattice parameter of 0.45 nm, *i.e.*, it was similar in structure to the MC phase. This phase appears to be a variant of the minor-phase Nb/Ni/Cr/Fe carbide phase seen in the base + B + P alloy. Similarly, another variation on the MC carbide was observed

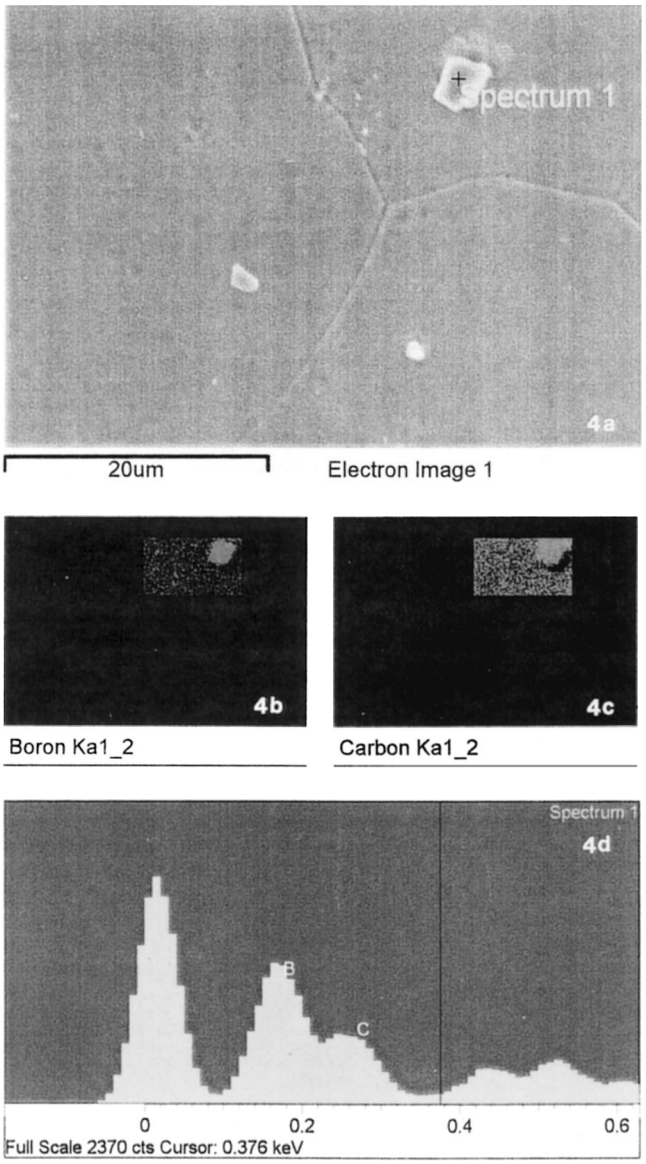

Fig. 4—(*a*) SEM micrograph of MC carbide from base + B + C alloy, (*b*) *x*-ray map of B, (*c*) *x*-ray map of C, and (*d*) portion of EDS spectrum of MC carbide in (a) showing B and C peaks.

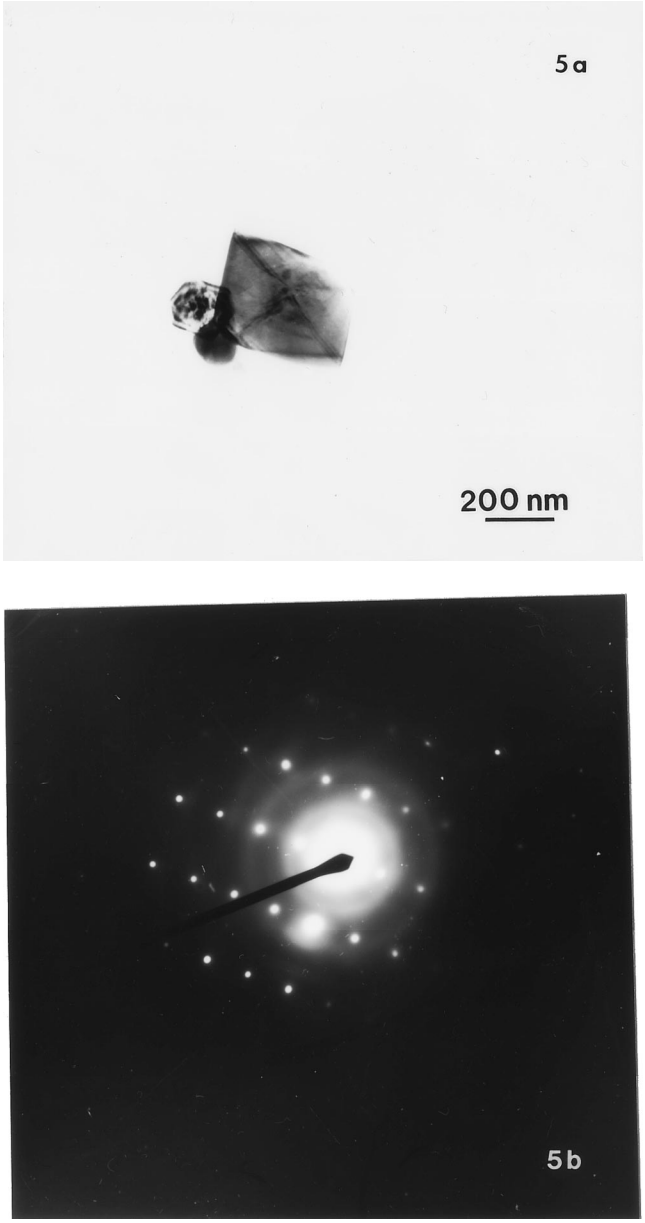

Fig. 5—(*a*) TEM micrograph of an extraction replica of base + B + C alloy showing MC type fcc carbide and (*b*) SAD pattern from MC carbide shown in (*a*) with [112] zone axis.

in the base + C + P alloy, being a Nb/Ti/Cr carbide (Table II) with the MC crystal structure.

Fine round/cuboid carbide particles (<1.0 μm) were observed in the base + B + C + P alloy, which were of the same Nb-rich MC type as in the base alloy, again containing Ti. These carbides were finer than those normally observed in INCONEL 718 without the P addition. It may be that the addition of P has modified the morphology of the carbides, resulting in finer and fewer carbides. No B or borides were observed in any of the EDS spectra from the carbides (Figures 8(a) and (b)) of the base + B + C + P alloy; however, some Ti-rich carbides were observed.

B. *Secondary Ion Mass Spectroscopy*

The SIMS analysis of the base and AC base + C alloy showed the presence of carbon in the primary precipitates (Figure 9(a)), corroborating the observations by the SEM and TEM. The analysis for B indicated minor grain-boundary segregation, but only in the AC alloy. Segregation of other elements such as Nb, Cr, Ni, *etc.*, was not observed.

The SIMS analysis of the AC base + B alloy revealed the presence of B in particles, as well as on grain boundaries (Figure 9(b)). However, the degree of segregation of B at grain boundaries was smaller in the water-quenched (WQ) specimens, as compared to the AC specimens, as was also observed in a previous study.[7,8,9] The base + B alloy also showed some C present as precipitates in the AC condition, similar to the SIMS image shown in Figure 9(a). Even in the WQ condition, the alloy still had some B segregation to grain boundaries as well as in precipitates (Figure 9(c)); again, a SIMS image for C in the base + B alloy in the WQ condition showed the presence of the element, as seen in Figure 9(a).

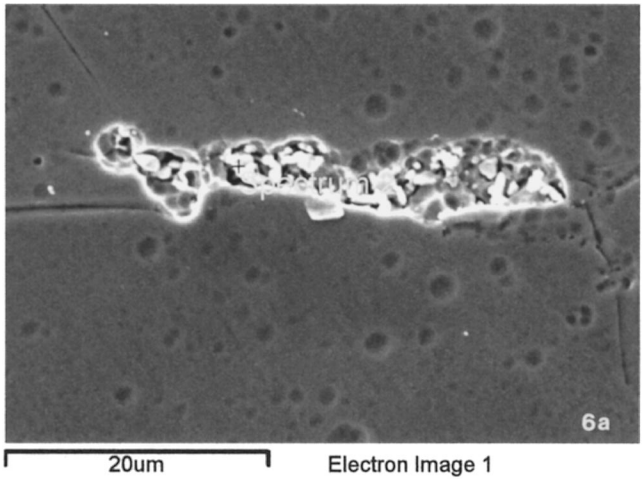

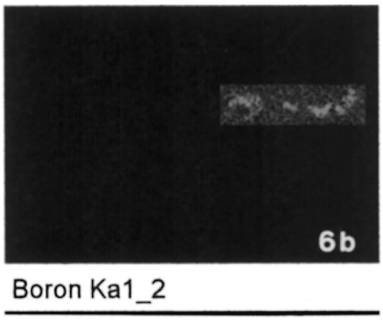

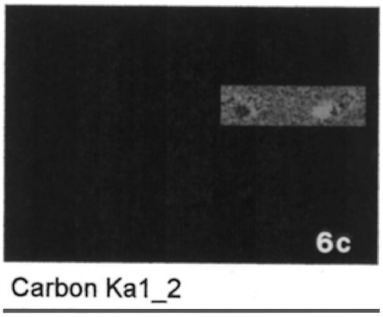

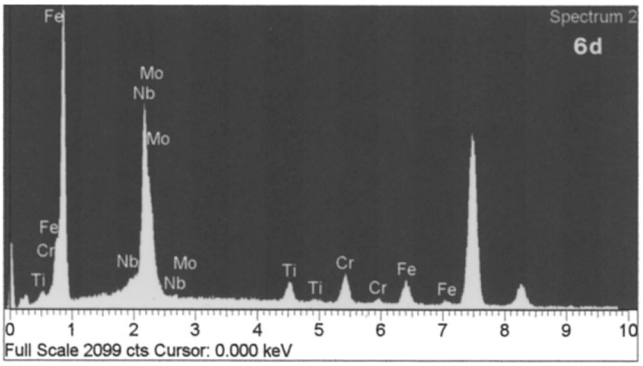

Fig. 6—(*a*) SEM micrograph showing grain boundary M_3B_2 borides in base + B + P alloy, (*b*) *x*-ray map of B, (*c*) X-ray map C, and (*d*) EDS spectrum of a boride precipitate in (a).

The base + C + B alloy showed only faint grain-boundary B images in the AC condition (Figure 9(d)), and no grain-boundary segregation was observed in the WQ samples (Figure 9(e)). It should be noted that the TEM studies did not reveal the presence of boride particles, and, thus, the

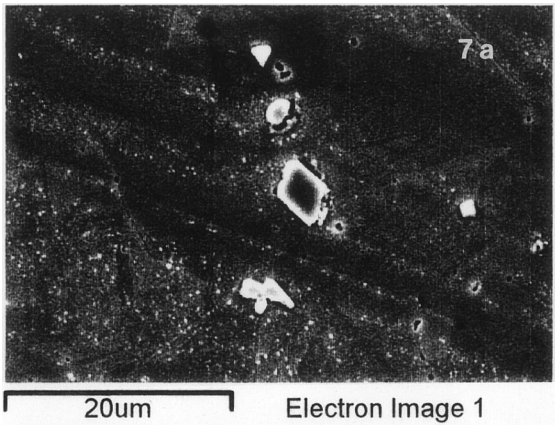

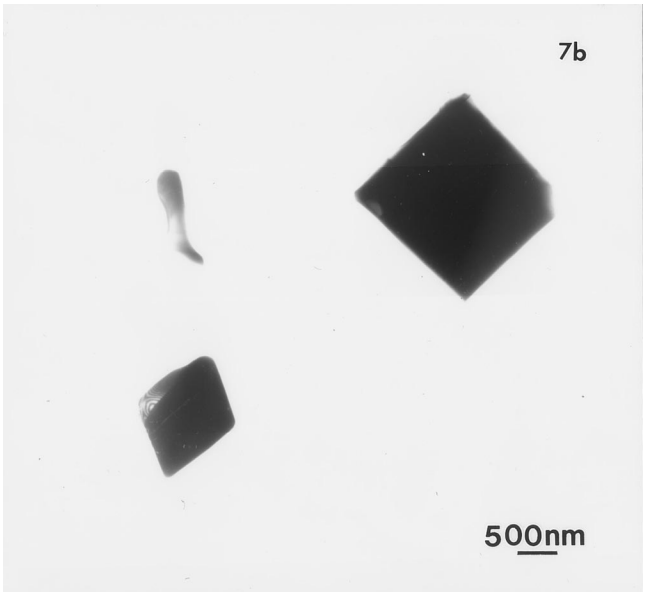

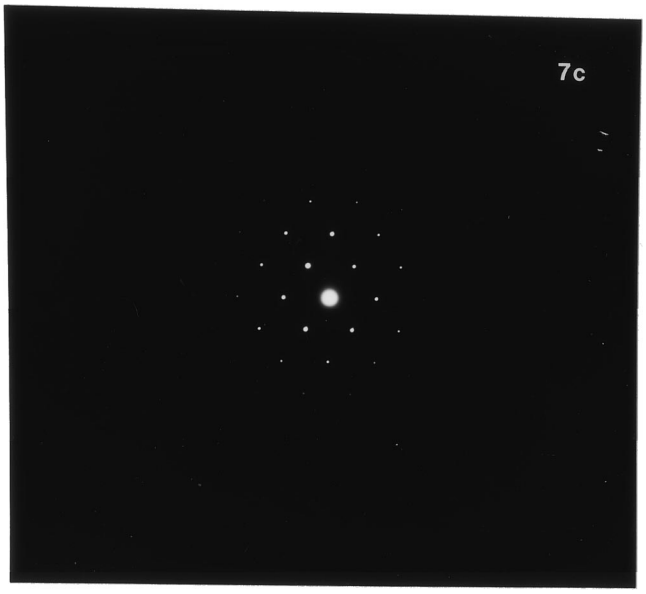

Fig. 7—(*a*) SEM micrograph of base + C + P alloy showing MC carbide, (*b*) TEM micrograph of extraction replica of a typical MC carbide shown in (a), and (*c*) SAD pattern of MC-type fcc carbide shown in (b) with [110] zone axis.

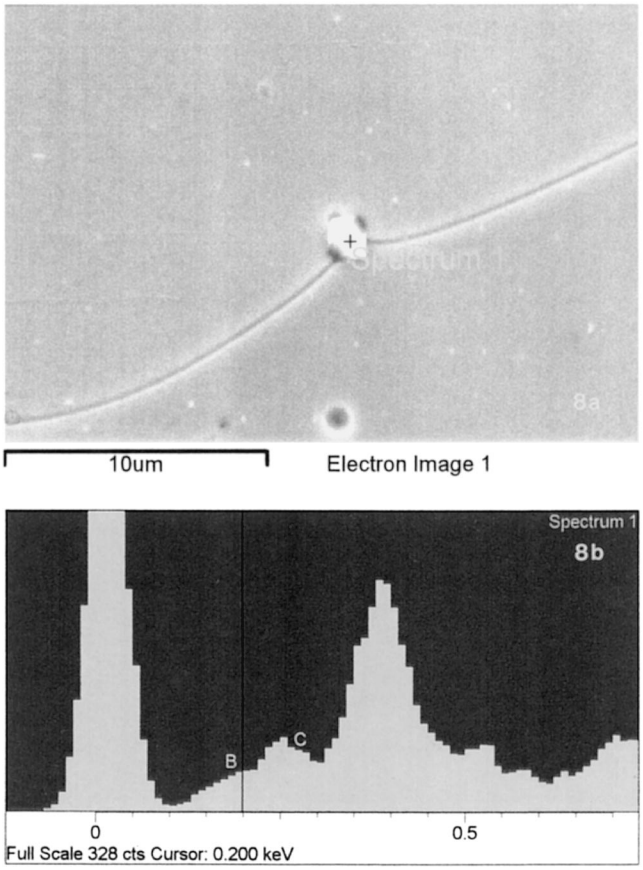

Fig. 8—(*a*) SEM micrograph of base + B + C + P alloy showing Nb-rich MC carbide. (*b*) portion of EDS spectrum of MC carbide in (a) showing C peak and absence of B peak.

majority of the B-ion images in Figure 9(d) are likely to be from Nb-rich carbide particles instead of boride particles. The SIMS images of C from the AC base + C + B alloy were similar to those of the base alloy (Figure 9(a)), with the C images emanating from MC carbides.

The base + B + P alloy in the AC condition showed segregation of B to the grain boundaries (Figure 9(f)), as well as in the precipitate particles. The SIMS analysis for P in the base + B + P alloy did not reveal any segregation of P, either to the grain boundaries or to the precipitate particles, although some P was detected in a few particles by SEM/EDS analysis. It is, therefore, possible that P was generally present as a monolayer in the grain boundaries but could not be detected by the SIMS used in this study. Horton *et al.*[19] detected segregation of B, C, and P to grain boundaries by the atom probe, but only a few M_3P precipitates of <50 nm in size were observed.

In the AC base + C + P alloy, only C showed strong images, as seen in Figure 9(a), again from MC carbide precipitates, with no P segregation being observed. Even though the B concentration in the alloy was less than 0.001 wt pct, some faint grain-boundary images were again observed (Figure 9(g)). In addition, some B segregation was observed to be associated with the carbide precipitates. This is corroborated by the SEM/EDS observations of B and C segregating to the precipitates.

In the AC base + B + C + P alloy, segregation of B occurred at the grain boundaries (Figure 9(h)), but only minor amounts of B-containing particles were observed. The SIMS analysis for C again showed a distribution similar to the one seen in Figure 9(a). In the WQ specimens, the segregation of B to carbides was also limited. This is consistent with the SEM/EDS observations, where only carbon was observed to be present in the particles and B was not observed.

C. *Hot Ductility Testing*

All seven alloys were evaluated in a Gleeble 1500 thermal simulator by the measurement of the ductility recovery temperature (DRT), where 5 pct reduction in area was used as a criterion for the ductility recovery. The effect of C, B, and P, individually and in combination with each other, on the weldability was analyzed by plotting the DRT values in four different graphs, shown in Figures 10(a) through (d). For a peak temperature of 1210 °C, the base alloy had the highest DRT temperature of 1200 °C, *i.e.*, its weldability was highest. On adding C, the DRT value was reduced by 20 °C to 40 °C, with the value of the AC specimens being slightly lower than that of the WQ specimens.

Upon the addition of B to the base + C alloy, the DRT values were reduced further by 60 °C to 80 °C. Again, the DRT value of the AC specimens was lower than that of the WQ specimens by a small, but noticeable, amount. The addition of P to the alloy containing C and B raised the DRT value of the AC specimens, but that of the WQ alloy remained almost unchanged.

The addition of P to the C-containing alloy (Figure 10(b)) had no influence on the DRT value of the AC specimens, but reduced the DRT of the WQ specimens from 1180 °C to 1100 °C. The addition of B to this alloy had no effect, even in the AC alloy.

Figure 10(c) shows the effect of B on the DRT value. The addition of B had the greatest influence, reducing the DRT value of the base alloy from 1200 °C to about 1090 °C in both the AC as well as WQ conditions. The addition of C to the B-containing alloy improved the DRT values by a small amount. The addition of P, however, to the B + C alloy resulted in DRT values which were mainly unaffected in the WQ condition and were improved in the AC condition.

The addition of P to the B-containing alloy reduced the DRT values to their lowest levels (Figure 10(d)). The ternary addition of C to the alloy improved the DRT values in both the WQ and AC specimens, with the improvement being greater in the AC specimen (Figure 10(d)).

These results suggest that the adverse effect of B on the DRT values and weldability is most severe. The addition of P to higher-B-containing alloys reduces the weldability even further. However, the addition of C to the B-containing alloy, as well as to the B + P–containing alloy, is beneficial, although when only C is present, the weldability of the B + P–free alloy is reduced to a small extent.

D. *Total Crack-Length Measurements*

The variation in the values of the Av. TCL by the additions of B, C, and P is shown in Figures 11(a) and (b). Generally, the Av. TCL measurements followed the same trend as observed in the DRT values (Figure 11(c)). The base alloy showed the lowest Av. TCL values, with a value

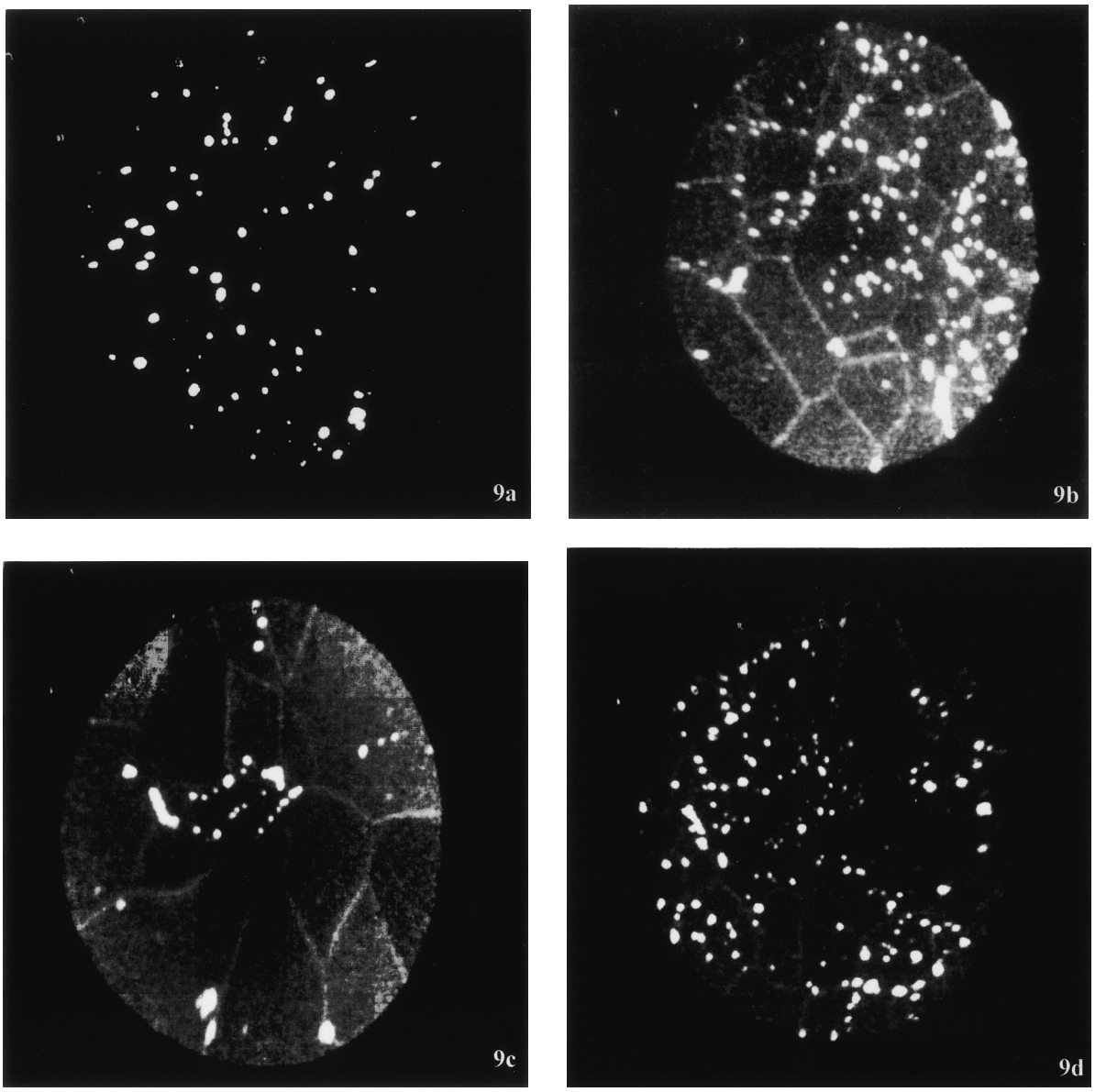

Fig. 9—SIMS images of base and B, C, and P containing alloys: (*a*) base alloy, AC, showing C in MC carbides; (*b*) base + B alloy, AC, showing B at GBs and in MC carbides; (*c*) base + B alloy, WQ, showing faint B image at GBs and in MC carbides; (*d*) base + B + C alloy, AC, showing faint B images at grain boundaries and B in MC carbides; (*e*) base + B + C, alloy WQ, showing the presence of B only in MC carbides; (*f*) base + B + P alloy, AC, showing B at grain boundaries and MC carbides, segregation of P was not observed by SIMS analysis; (*g*) base + C + P alloy, AC, showing the presence of B at GBs and in MC carbides; and (*h*) base + B + C + P alloy, AC, showing B at GBs and in MC carbides.

of 24 μm. The addition of C did not significantly affect the Av. TCL value in either the AC or WQ condition. In contrast, the addition of B increased the Av. TCL values to 105 and 72 μm in the AC and WQ conditions, respectively.

On the addition of B to the base + C alloy, the Av. TCL values were increased in both the AC and WQ conditions, while the effect of the addition of P was influenced by the cooling rate (Figure 11). From this figure, it can be seen that in the sequence (base, base + C, base + C + P, and base + C + P + B) there is an increase in the Av. TCL up to the B + P alloy, then a decrease with additions of C. Alternatively, considering the sequence of alloys (base, base + B, base + B + P, and base + B + P + C), the detrimental effect of P is evident when C is low (Figures 11(a) and (b)), in both the AC and WQ conditions. When C is present (Figures 11(a) and (b)), the detrimental effect of P is mitigated, as also demonstrated by hot ductility measurements.

IV. DISCUSSION

A. *Segregation Behavior*

The segregation behavior of B, C, and P can be rationalized by considering the driving force for segregation, the free energy for grain-boundary segregation (ΔG_s), and the potential competition between the segregating species. In addition, the activity of segregating species such as C can also influence segregation behavior, depending on the actual concentration present.

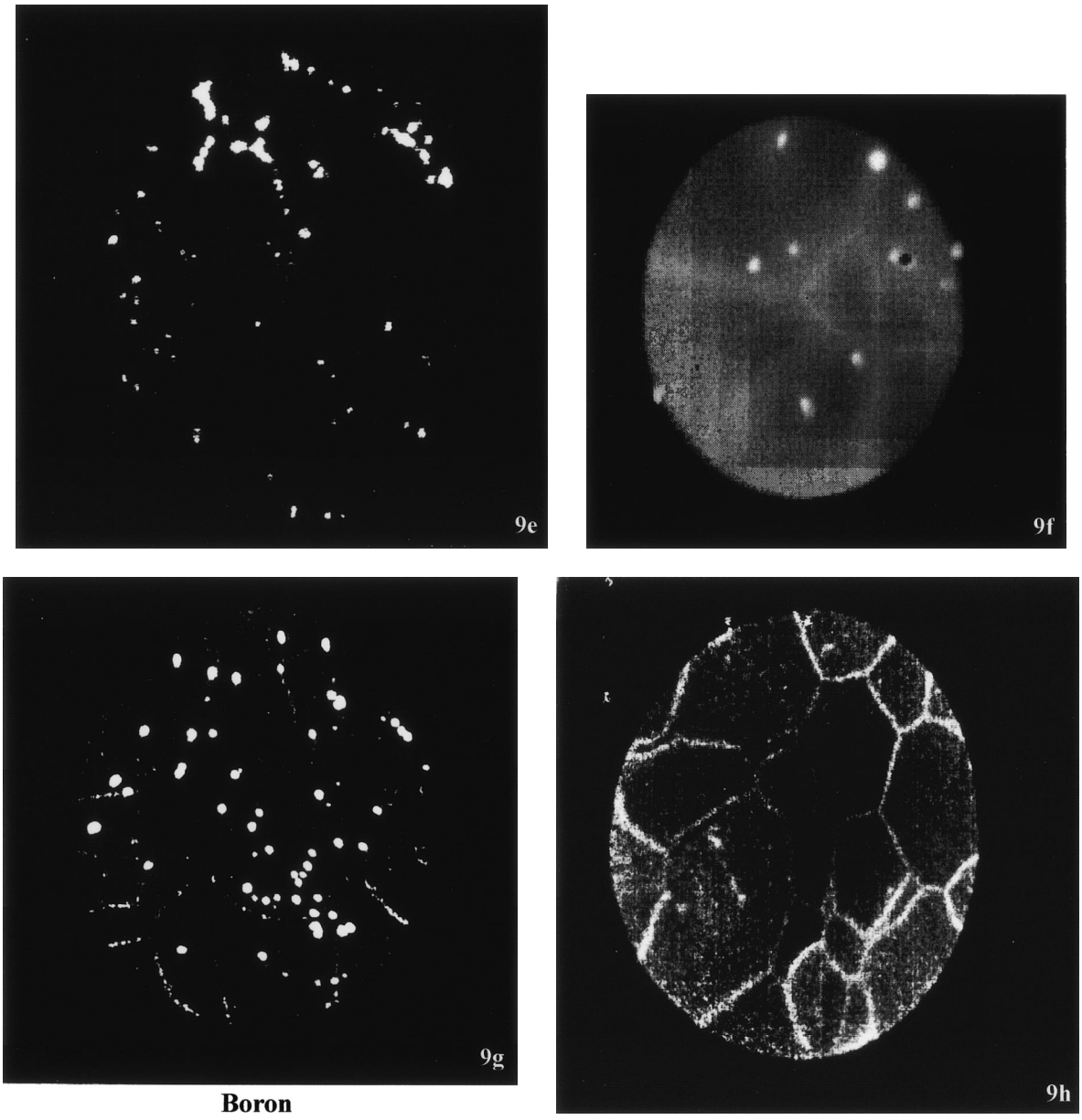

Fig. 9—Continued. SIMS images of base and B, C, and P containing alloys: (*a*) base alloy, AC, showing C in MC carbides; (*b*) base + B alloy, AC, showing B at GBs and in MC carbides; (*c*) base + B alloy, WQ, showing faint B image at GBs and in MC carbides; (*d*) base + B + C alloy, AC, showing faint B images at grain boundaries and B in MC carbides; (*e*) base + B + C, alloy WQ, showing the presence of B only in MC carbides; (*f*) base + B + P alloy, AC, showing B at grain boundaries and MC carbides, segregation of P was not observed by SIMS analysis; (*g*) base + C + P alloy, AC, showing the presence of B at GBs and in MC carbides; and (*h*) base + B + C + P alloy, AC, showing B at GBs and in MC carbides.

Paju[16] considered the segregation behavior of B, C, and P in austenite. The ΔG_s values for B, P, and C were −97, −47 to −53, and −30 kJ/mol, respectively. In the presence of B, however, the P free-energy value was reduced *via* a site-competition effect from an original value of −50.5 kJ/mol to −43.5 kJ/mol. Similarly, the P concentration in austenite was reduced by C additions *via* site competition, although a less-strong effect was observed in the case of C influencing P segregation than with B. Thus, B is the most likely segregating species, as shown by the SIMS results, with B being more potent in displacing P from grain boundaries than C. Similar behavior for C displacement of P in austenite has been postulated by Glickman *et al.*[20] and observed by Erhart and Grabke.[13] The ΔG_s value for C reported by Erhart and Grabke was −76 kJ/mol, which is considerably higher than Paju's data, but would fit the trend of C displacing P.

The effect of the additions of C, B, and P as individual elemental additions and in combinations of elements on weldability will be discussed in three groups, based on the free-energy data given previously, *i.e.*, as an individual effect, the interaction of two elements, and, finally, as the influence of three elements.

B. *Individual Effect*

As shown in Figures 11(a) and (b), the effect of C can be understood by evaluating the base alloy with that of the base + C alloy. A carbon addition to the base alloy increased the volume fraction of carbides, although the overall increase

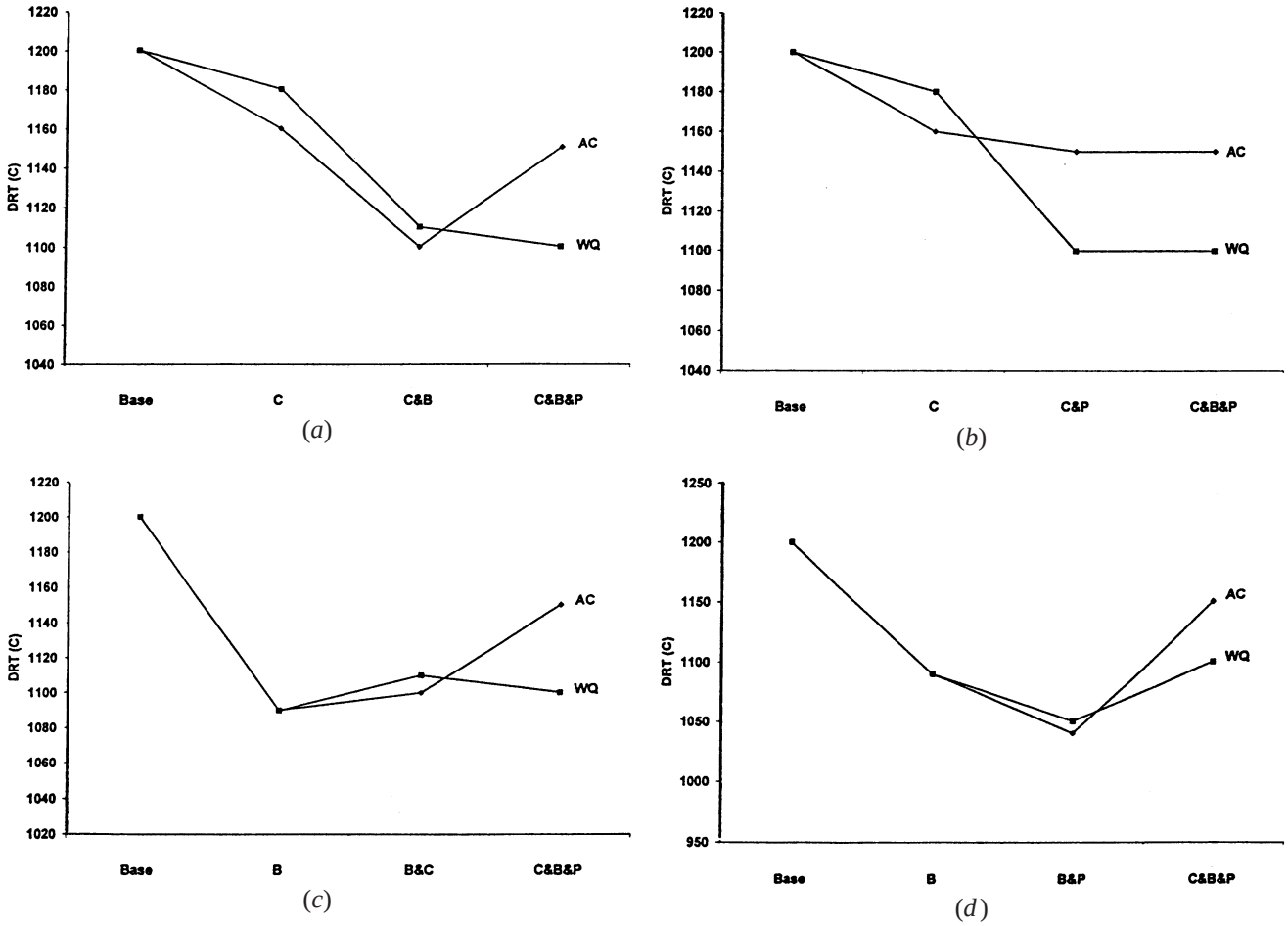

Fig. 10—Variation in the value of DRT by the addition of (*a*) C, B, and P; (*b*) C, P, and B; (c) B, C, and P; and (*d*) B, P, and C.

in C from 0.008 to 0.03 wt pct had limited effect on the Av. TCL values. It is likely that the extra amount of carbide with the 0.03 wt pct addition would have little effect on the Av. TCL values, since the volume fraction of carbide is still only about 1.5 pct. These observations are in agreement with Kelly's research[5] on the cast alloy INCONEL 718, where he showed that C additions of up to 0.1 wt pct had no effect on the TCL values. Previous work by Thompson *et al.*,[2] on the other hand, found that the TCL values increased by 24 pct in cast INCONEL 718 on raising the C level from 0.02 to 0.06 wt pct.

An understanding of the influence of B can be obtained from Figures 11(a) and (b), by comparing the base alloy to the base + B alloy, where a considerable increase in Av. TCL values occurred. The addition of B led to the precipitation of boride particles in the solution-treated condition and to significant segregation of B to the grain boundaries, especially in the AC condition. This modification of the microstructure affected the ductility of the material. The base + B alloy showed increased microfissures after electron-beam welding (Figures 11(a) and (b) compared to the base alloy, especially in the AC specimen, and a low DRT value in Gleeble testing (Figures 10(c) and (d)). The segregation of B on grain boundaries lowered the solidification temperature of the boundaries and led to the formation of microfissures due to cooling stresses after welding.[7,8,9]

Therefore, it can be seen that B has a detrimental effect on the weldability of INCONEL 718, as demonstrated through its adverse influence on the Gleeble hot-ductility DRT parameter and the Av. TCL values.

C. *Interaction of Two Elements*

1. *Carbon-boron*

The effect of the C and B additions on weldability can be evaluated by considering the DRT and Av. TCL values of the base, base + B, and base + C + B alloys. As shown in Figures 10 and 11, the addition of B to the base + C alloy resulted in a reduction in the value of DRT and a general increase in the Av. TCL values, *i.e.*, both values were detrimentally affected. The addition of C to the B alloy showed a slight improvement in the DRT value and a moderate improvement in the Av. TCL values (*i.e.*, an improvement in weldability). The detrimental influence of the addition of B on the weldability parameters of the base + 0.03 pct C alloy is related to boron's well-known effect in reducing weldability, as reported in earlier studies[7,8,9] and outlined in the previous section. Thus, B exacerbates the effect of C additions from values as low as possible to up to about 0.1 wt pct, *via* a combination of equilibrium and nonequilibrium segregation.

Since the C addition is not large enough to affect the solidification path (with greater than about 0.1 wt pct being needed, according to Dupont *et al.*[21]), from the free-energy data, it is likely that C can compete with B for grain-boundary sites and, thus, mitigate to some extent the deleterious effect

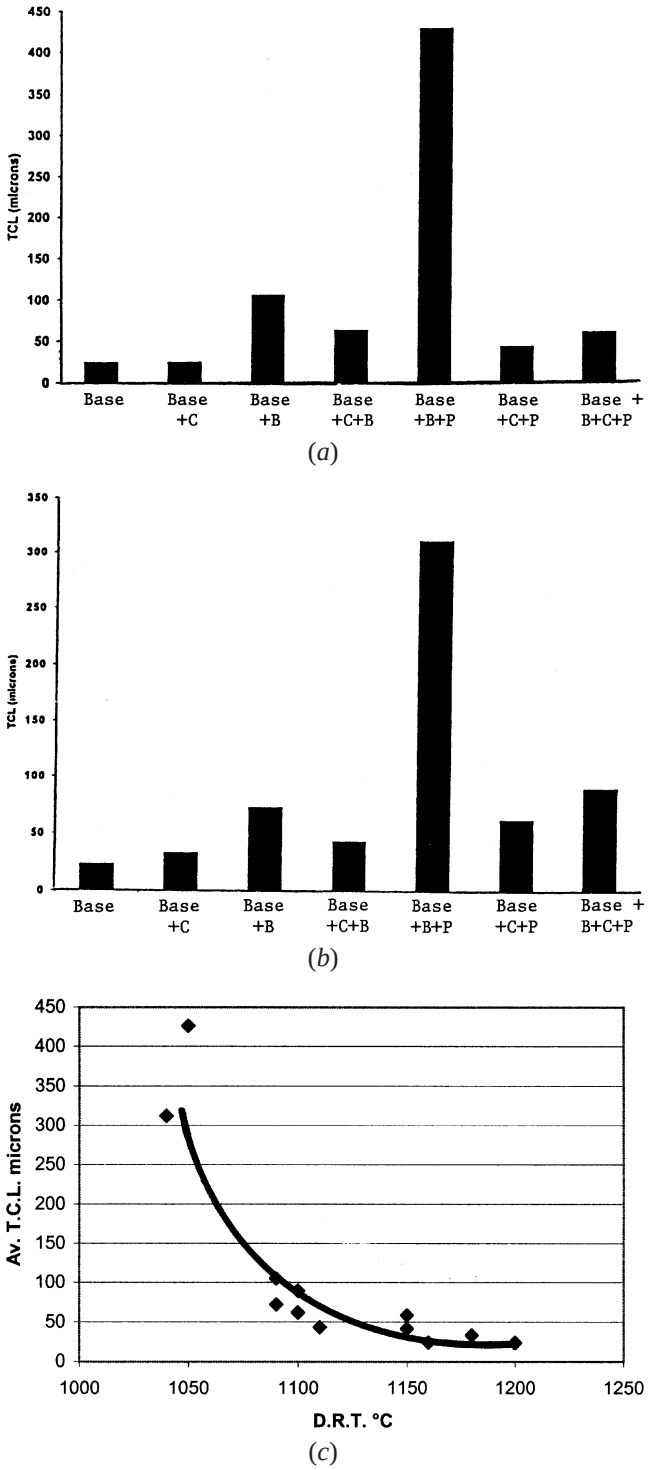

Fig. 11—Values of Av. TCL in different alloys in the (*a*) AC and (*b*) WQ condition and (c) correlation between Av. TCL and DRT values.

of B. Furthermore, with more carbides present, some B is incorporated into the carbides and, consequently, reduces the concentration of B on the grain boundaries, thus reducing its deleterious effect on the weldability of the alloy. There was no indication of the presence of any borides in the microstructures of any of the alloys that contained 0.03 wt pct C.

2. *Carbon-phosphorous*

The weldability data from the base + C and base + C + P alloys showed the effect of the C and P additions. The DRT values were variably affected depending on cooling rate (Figure 10(b)), whereas the TCL value was adversely affected by the P addition (Figures 11(a) and (b)). The microstructure of the base + C + P alloy contained the usual Nb-rich MC carbide with some Ti, but no new precipitates such as phosphide were observed; furthermore, P was not detected on the grain boundaries by SIMS analysis. It may be that P segregated to the boundaries as a monolayer, which would be difficult to detect by SIMS. As shown earlier from free-energy-of-segregation data, Paju[14,15,16] observed that C affected the segregation of P in austenite by mutual displacement, with both elements segregating to grain boundaries. Similar results were obtained by Erhart and Grabke,[13] where it was also proposed that a sufficient activity of C could displace P from grain boundaries, even in a high-P material. Consequently, in an alloy containing a sufficient level of C, as in the base + C + P alloy, the effect of P is likely to be mitigated by the presence of 0.03 wt pct C.

3. *Boron-phosporous*

A comparison of the base + B and base + B + P alloys illustrates the effect of the addition of P to a B-containing alloy in the presence of low C. The P addition to the high-B alloy dramatically increased the Av. TCL values by factors of 3 and 6 in the AC and WQ alloys, respectively, and reduced the DRT values by 40 °C to 50 °C, to the lowest values observed during the whole investigation. The base + B + P alloy, which contained B and P coupled with a low C level, also contained the Nb/Mo/Cr boride, which was observed to be detrimental to the microfissuring resistance of the alloy (Figures 10(d) and 11 (a) and (b)). As is to be expected, if nonequilibrium segregation was occurring, the SIMS image for B would be stronger in the AC than in the WQ condition, as was the case; however, the SIMS analysis did not show any segregation of P. Again, the P may be segregating by equilibrium segregation or the B may be influencing its grain-boundary segregation. This has been also observed by Paju *et al.*[14,15,16] where B additions were found to reduce the segregation of P to grain boundaries in accordance with the higher ΔG_s value for B with respect to P. In the present study, however, the combination of P and B in a low-C alloy was observed to be detrimental to weldability, showing the worst combination of DRT values and the highest Av. TCL values for the entire experimental set.

D. *Interaction of Three Elements*

The combination of the effect of the three minor-element additions of C, B, and P on the DRT and Av. TCL values is seen by comparing the behavior of the base + B + C + P alloy to that of the base + B + P alloy. The most dramatic effect of the three-element combination is seen in Figures 11(a) and (b), where the addition of 0.03 wt pct C in the base + B + P alloy reduced the Av. TCL values from the B + P alloy by a factor of about 0.8 in both the AC and WQ conditions. Similarly, the DRT values improved by 50 °C to 110 °C for the AC and WQ conditions (Figure 10(d)). The microstructure of the base + B + C + P alloy showed only fine carbides, in contrast to the base + B + P alloy, where borides were observed. The location of the borides on the grain boundaries in the base + B + P alloy considerably influenced both of the weldability parameters. The addition of C, however, in the base + B + P + C alloy eliminated

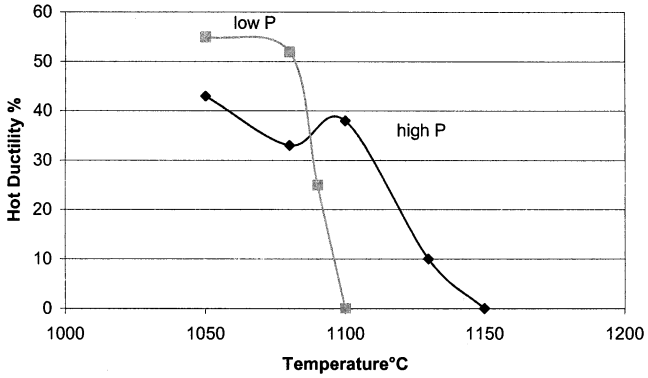

(*a*)

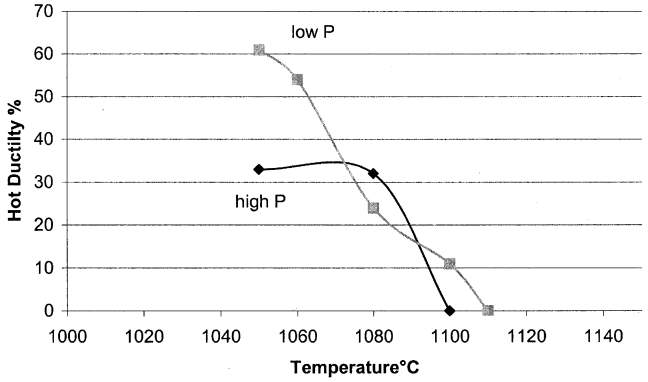

(*b*)

Fig. 12—Effect of P addition on the hot ductility values of C + B alloy in (*a*) AC and (*b*) WQ condition.

the presence of the borides and considerably improved the weldability of the alloy.

The reason why the addition of C influences the behavior of P can be understood from the observations of Paju *et al.*[14,15,16] and Erhart and Grabke,[13] as mentioned earlier. To this effect, one can assume that the 0.03 wt pct C addition was sufficient to reduce segregation of P on grain boundaries to a level where the precipitation of borides and/or phosphides was prevented. Segregation of P was not observed in the SIMS analysis, but it is likely, however, that some P segregation still exists in the alloy, although its effect is likely to be severely mitigated by the C activity arising from the 0.03 wt pct addition. As mentioned previously, Horton *et al.*[19] have observed C, B, and P elemental segregation to the grain boundaries of modified alloy 718, using the atom probe. From the present Gleeble data (Figures 12(a) and (b)), P is seen to have an effect on the hot-ductility values of the base + C + B and base + B + C + P alloys in the AC condition, but not in the WQ state. This effect, also shown in Figure 10(a), demonstrates that during air cooling a likely P segregation effect occurs, since the DRT values of the AC specimens, as compared against those of the WQ specimens, are considerably at variance. In Figure 10(a), for example, the DRT values of the AC base + C + B alloy and the base + B + C + P alloy differ by some 50 °C; in the WQ alloys, the difference is only 10 °C; and also, as can be seen from Figure 10(a), the P addition is beneficial to the DRT value in the AC condition only. This segregation effect is likely to be a fine-scale segregation of P, as shown by Horton *et al.*[19] In the base + C + B alloy, there may be sufficient C present to site compete with the P and, thus, to displace the P, but, in the base + B + C + P alloy, the P activity level may be sufficient to actively compete with the C (and/or B) for grain-boundary sites.

In addition to the free-energy-based analysis presented in this communication, Chen *et al.*[22] have considered the kinetics of segregation under similar cooling rates and found significant B segregation during the thermal cycles experienced by the alloys. The reader is referred to that article for details.

In conclusion, it is suggested that in INCONEL 718–based alloys, segregation of B during preweld solution treatment changes the local chemistry of GBs, which leads to HAZ microfissuring. However, the segregation of B is influenced by the interaction among C, P, and B through grain-boundary site competition, which affects the weldability of the alloy.

V. SUMMARY AND CONCLUSIONS

1. Additions of C, B, and P, either individually or in combinations, can strongly influence the weldability of INCONEL 718.
2. The addition of 0.03 wt pct C to a base alloy containing 0.008 wt pct C showed little effect on the Av. TCL values, but reduced the DRT value by up to 40 °C in the AC condition.
3. On the other hand, the addition of B to the base alloy had an adverse effect on both the Av. TCL and DRT values.
4. An addition of C to the B-containing alloy somewhat mitigated the detrimental effects of B. This can be explained by the GB site competition among the segregating species.
5. A B + P combination adversely influenced the Av. TCL and DRT values significantly, through the formation of borides; in addition, their location on grain boundaries increased the effect on weldability.
6. As in the case of the B-containing alloy, the addition of C to a P-containing alloy reduced the adverse effect of P, which could also be attributed to the site competition among the minor elements.
7. Similarly, in a C + P + B alloy, C mitigated the detrimental effects of B and P through the elimination of borides and some of the B being incorporated into the Nb-rich carbides.
8. Borides were not observed in the microstructure when C was present.

ACKNOWLEDGMENTS

The authors thank the Natural Sciences and Engineering Research Council of Canada and a consortium of Manitoba aerospace industries for the financial support. The authors are extremely grateful to Dr. W.D. Cao and Allvac for providing the material, to Dr. G. McMahon, Materials Technology Laboratory of CANMET (Ottawa) for the SIMS analysis. Thanks are also due to Ms. U. Prasad and Dr. Q. Xu, Industrial Technology Centre (Winnipeg), for their assistance with the TEM analysis.

REFERENCES

1. W.A. Owczarski, D.S. Duvall, and C.P. Sullivan: *Weld. J.*, 1966, vol. 45 (4), p. 145-s.
2. R.G. Thompson, D.E. Mayo, and B. Radhakrishnan: *Metall. Mater. Trans. A*, 1991, vol. 22A, pp. 557-67.
3. R.G. Thompson, J.R. Dobbs, and D.E. Mayo: *Weld. J.*, 1986, vol. 65, p. 299-s.
4. R.G. Thompson, B. Radhakrishnan, and D.E. Mayo: *J. Phys.*, 1988, Coll. C5, suppl. 10, Tome 49, p. C5-471.
5. T.J. Kelly: *Adv. Weld. Sci. Technol.*, 1986, p. 623.
6. W.F. Savage, E.F. Nippes, and G.M. Goodwin: *Weld. J.*, 1977, Aug, p. 245-s.
7. X. Huang, N.L. Richards, and M.C. Chaturvedi: *3rd Int. SAMPE Metals and Metals Processing Conf.*, F. Froes, W. Wallace, R. Cull, and E. Struchholt, eds., SAMPE, Toronto, 1992, pp. M231-M242.
8. X. Huang, N.L. Richards, and M.C. Chaturvedi: *Metall. Trans. A*, 1996, vol. 27A, p. 785.
9. X. Huang, M.C. Chaturvedi, N.L. Richards, and J. Jackman: *J. Acta Mater.*, 1997, vol. 48, p. 3095.
10. H. Guo, M.C. Chaturvedi, and N.L. Richards: *Sci. Technol. Weld Join*, 2000, vol. 5 (6), p. 1718.
11. W.D. Cao, and R.L. Kennedy: in *Superalloys 718, 625, 706 and Various Derivatives*, E.A. Loria, ed., TMS, Warrendale, PA, 1994, p. 463.
12. M.H. Guttman: *Phil. Trans. R. Soc.*, 1980, vol. A295, p. 169.
13. H. Erhart and H.J. Grabke: *Met. Sci.*, 1981, vol. 15, p. 401.
14. M. Paju and R. Moller: *Scripta Metall.*, 1984, vol. 18, p. 813.
15. M. Paju and H.J. Grabke: *Mater. Sci. Technol.*, 1989, vol. 5, p. 148.
16. M. Paju: Ph.D. Thesis, Helsinki University of Technology, Helsinki, 1990.
17. N.L. Richards and M.C. Chaturvedi: *Int. Mater. Rev.*, 2000, vol. 45 (3), p. 109.
18. R. Vincent: *Acta Metall.*, 1985, vol. 33 (7), p. 1205.
19. J.A. Horton, C.G. McKamey, and M.K. Miller: *Superalloys 718, 625, 706 and Various Derivatives*, E.A. Loria, ed., TMS, Warrendale, PA, 1997, p. 401.
20. Y.E. Glickman, V.F. Kotyshev, Y.I. Cherpakov, and R.E. Bruver: *Phys. Met. Metallogr.*, 1973, vol. 36, p. 126.
21. N. Dupont, C.V. Robino, and A.R. Marder: *Weld. J.*, 1998, Oct., p. 417-S.
22. W. Chen, M.C. Chaturvedi, and N.L. Richards: *Metall. Mater. Trans. A*, 2001, vol. 32A, p. 931.